Creation of topological states of a Bose-Einstein condensate in a square plaquette of four optical traps

Tomasz Świsłocki,[1] Tomasz Sowiński,[1] Mirosław Brewczyk,[2] and Mariusz Gajda[1]
[1]*Instytut Fizyki PAN, Al.Lotników 32/46, PL-02-668 Warsaw, Poland*
[2]*Wydział Fizyki, Uniwersytet w Białymstoku, ul. Lipowa 41, PL-15-424 Białystok, Poland*
(Received 13 August 2010; revised manuscript received 18 May 2011; published 16 August 2011)

We study a square plaquette of four optical microtraps containing ultracold ^{87}Rb atoms in the $F = 1$ hyperfine state. In the presence of an external resonant magnetic field, the dipolar interactions couple the initial $m_F = 1$ component to other Zeeman sublevels. This process is a generalization of the Einstein–de Haas effect to the case when the external potential has only C_4 point symmetry. We observe that vortex structures appear in the initially empty $m_F = 0$ state. Topological properties of this state arise due to competition between the local axial symmetry of the individual trap and the discrete symmetry of the plaquette. For deep microtraps vortices are localized at individual sites, whereas for shallow traps only one discrete vortex appears in the plaquette. States created in these two opposite cases have different topological properties related to C_4 point symmetry.

DOI: 10.1103/PhysRevA.84.023625 PACS number(s): 03.75.Mn, 05.30.Jp, 75.45.+j, 75.50.Mm

I. INTRODUCTION

Experimental achievements in cooling alkali-metal atoms provide multiple possibilities to explore Bose-Einstein condensation phenomena. The first Bose-Einstein condensates were created in magnetic traps and allowed the study of properties related to weak contact interactions in atomic condensates. Not long after, optical confinement of ultracold atoms became possible, and new systems—spinor condensates—were realized. There, the ability to simultaneously trap atoms in many magnetic states makes it possible to investigate nontrivial spin dynamics and magnetism in ultracold Bose gases. They have already been studied both experimentally and theoretically [1–6].

It was realized quite early that dipolar interactions between ultracold species might lead to many novel phenomena [7–9]. The interesting features of dipolar interactions are rooted in their long range as well as anisotropic character. After many years of experimental struggle, a Bose-Einstein condensate of ^{52}Cr atoms whose magnetic dipole moment equals $6\mu_B$ was obtained [10,11]. This achievement opened the possibility to study a variety of phenomena related to dipolar interactions [12,13]. Some authors [6,14–17] noticed, however, that magnetic dipole interactions might lead to observable effects even in a gas of rubidium atoms. An example is the Einstein–de Haas effect [17,18] (studied also for ^{52}Cr condensate in [19]). The main concept is that rubidium atoms trapped initially in the $m_F = +1$ component can be efficiently transferred to the $m_F = 0$ state and then further to the $m_F = -1$ Zeeman sublevel. This can happen only if the external magnetic field is tuned to a resonant value. Moreover, atoms in the $m_F = 0$ and $m_F = -1$ states acquire one or two quanta of orbital angular momentum, respectively [17].

The ability to use interfering laser beams to create optical lattices filled with ultracold bosonic or fermionic atoms has opened new possibilities. Atomic physics began to penetrate areas traditionally associated with solid-state physics. The observation of the Mott-insulator–superfluid transition in an optical lattice [20–22] was a very important step toward the investigation of strongly correlated systems described by various Hubbard-type Hamiltonians. Subsequently, degenerate gases in optical lattices are being studied very intensively [23,24].

Progress in experimental techniques has allowed the creation of new types of optical lattices, such as superlattices or arrays of coupled plaquettes [25]. In this article we focus on topological states of an ultracold atomic system in a single plaquette. We study the case of a relatively highly occupied plaquette, which allows for a mean-field description of the system. Such systems are experimentally accessible [26,27]. We concentrate on the topological phases of the macroscopic order parameter. Creation of these dynamical states implicitly utilizes the dipolar interactions tuned by the external magnetic field. An external magnetic field is a perfect tool for manipulating the system in the controlled manner. The analysis presented in this article becomes especially important in the context of a recent experiment [27] aimed at the observation of the Einstein–de Haas effect in a chromium condensate in an optical lattice.

If the atoms are located in an array of traps, then the Einstein–de Haas effect may exhibit new interesting aspects. Conservation of the total angular momentum is the essence of the Einstein–de Haas effect. In this article we assume that ^{87}Rb atoms are placed in a square plaquette of four optical traps. Therefore, the external potential has no axial symmetry, and the z component of the total angular momentum does not have to be conserved. Instead, the C_4 point symmetry comes into play. The aim of this article is to investigate the role of this symmetry in the dynamics driven by the dipolar interactions. The relative weight of the local axial symmetry of the trap and the discrete symmetry of the plaquette can be controlled by varying the height of the barrier separating the traps.

This paper is organized as follows. In Sec. II we describe the system under consideration. In particular, we discuss in detail the properties of dipolar interactions which are essential for the physics reported in the article. Section III presents numerical results regarding the Einstein–de Haas effect for a rubidium condensate in a plaquette whereas Sec. IV explains why dipolar

resonances sometimes lead to a global discrete vortex state while in other situations to an array of local vortices. In Sec. V we discuss the stability of the states obtained via the resonant Einstein–de Haas effect. We end with conclusions in Sec. VI.

II. DESCRIPTION OF THE SYSTEM

The single-particle Hamiltonian has the following form:

$$H_0 = \int d\mathbf{r}\ \hat{\psi}^\dagger(\mathbf{r}) \left(\frac{\mathbf{p}^2}{2m} + V_{tr}(\mathbf{r}) - \gamma\, \mathbf{B}\hat{\mathbf{F}} \right) \hat{\psi}(\mathbf{r}), \qquad (1)$$

where $\hat{\psi}(\mathbf{r}) = (\hat{\psi}_+(\mathbf{r}), \hat{\psi}_0(\mathbf{r}), \hat{\psi}_-(\mathbf{r}))^T$ is the spinor annihilation operator, $\hat{\mathbf{F}} = (\hat{F}_x, \hat{F}_y, \hat{F}_z)$ are standard $F = 1$ spin matrices, and γ is the gyromagnetic coefficient. The external potential of the plaquette V_{tr} is

$$V_{tr}(\mathbf{r}) = V_0[\cos^2(k_0 x) + \cos^2(k_0 y)] + \tfrac{1}{2} m[\omega_\perp^2 (x^2 + y^2) + \omega_z z^2]\,. \qquad (2)$$

The first term describes a periodic lattice, while the second one corresponds to a relatively weak harmonic potential. This harmonic confinement is essential to consider the stability of topological states created by the resonant Einstein–de Haas effect (Sec. V). Otherwise (Secs. III and IV), we assume that only the axial (i.e., along the z axis) part of harmonic trapping is present. The lattice is defined on a square section of the xy plane centered at $x = y = 0$ and containing four lattice minima which form a square and are separated by $d_0 = \pi/k_0$. V_0 is a potential barrier separating lattice sites. The last term in Eq. (1) is responsible for the linear Zeeman shift due to a uniform magnetic field $\mathbf{B}$ directed along the z axis. In what follows, we assume that the magnetic field is weak and therefore the quadratic Zeeman effect can be neglected.

The short-range interactions are typically described by a pseudopotential. In the case of a spinor $F = 1$ condensate, this interaction can be split into the spin-independent term proportional to $c_0 = 4\pi\hbar^2(2a_2 + a_0)/(3m)$ and the spin-dependent part proportional to $c_2 = 4\pi\hbar^2(a_2 - a_0)/(3m)$ [28], where a_2 (a_0) is a scattering length of two colliding atoms with total spin $F = 2$ ($F = 0$). The Hamiltonian describing the short-range interactions can be written in the form:

$$H_C = \int d\mathbf{r}\ \left(\frac{c_0}{2} :n^2(\mathbf{r}): + \frac{c_2}{2} :\mathbf{F}^2: \right), \qquad (3)$$

where $n(\mathbf{r}) = \sum \psi_s^\dagger \psi_s$ is the total atom density, :: denotes normal ordering, and the square of the total spin operator can be written as $\mathbf{F}^2(\mathbf{r}) = 2\,[F_+(\mathbf{r})F_-(\mathbf{r}) + F_-(\mathbf{r})F_+(\mathbf{r})] + F_z(\mathbf{r})F_z(\mathbf{r})$. The raising (lowering) operators of the z component of the spin of the atom at position $\mathbf{r}$ are defined as

$$F_\pm(\mathbf{r}) = \hat{\psi}^\dagger(\mathbf{r})\, \frac{\hat{F}_x \pm i\hat{F}_y}{2}\, \hat{\psi}(\mathbf{r}), \qquad (4)$$

while the magnetization density is

$$F_z(\mathbf{r}) = \hat{\psi}^\dagger(\mathbf{r})\, \hat{F}_z\, \hat{\psi}(\mathbf{r}). \qquad (5)$$

Finally, the long-range dipolar Hamiltonian is

$$H_D = \frac{\gamma^2}{2} \int d\mathbf{r} \int d\mathbf{r}' :\frac{\mathbf{F}(\mathbf{r})\mathbf{F}(\mathbf{r}') - 3[\mathbf{F}(\mathbf{r})\mathbf{n}][\mathbf{F}(\mathbf{r}')\mathbf{n}]}{|\mathbf{r} - \mathbf{r}'|^3}:, \qquad (6)$$

where $\mathbf{n}$ is a unit vector in the direction of $\mathbf{r} - \mathbf{r}'$. Using the explicit form of spin-1 matrices, the above Hamiltonian can be brought to the form:

$$H_D = \frac{1}{2} \int d\mathbf{r} \int d\mathbf{r}' \frac{\gamma^2}{|\mathbf{r} - \mathbf{r}'|^3} :h_D(\mathbf{r}, \mathbf{r}'):, \qquad (7)$$

where $h_D(\mathbf{r}, \mathbf{r}')$ has the form:

$$\begin{aligned} h_D = {} & A\,[F_z(\mathbf{r}')F_z(\mathbf{r}) - F_+(\mathbf{r}')F_-(\mathbf{r}) - F_-(\mathbf{r}')F_+(\mathbf{r})] \\ & - 3\sin^2\theta [e^{-2i\phi} F_+(\mathbf{r}')F_+(\mathbf{r}) + e^{2i\phi} F_-(\mathbf{r}')F_-(\mathbf{r})] \\ & - 3/2 \sin 2\theta\, e^{-i\phi} [F_+(\mathbf{r}')F_z(\mathbf{r}) + F_z(\mathbf{r}')F_+(\mathbf{r})] \\ & - 3/2 \sin 2\theta\, e^{i\phi} [F_z(\mathbf{r}')F_-(\mathbf{r}) + F_-(\mathbf{r}')F_z(\mathbf{r})]. \end{aligned} \qquad (8)$$

θ and ϕ are the spherical coordinate angles of the vector $\mathbf{r} - \mathbf{r}'$ connecting two interacting atoms, and $A = 1 - 3\cos^2\theta$. The form of Eq. (8) facilitates a physical interpretation of all terms. The first line represents dipolar interactions which do not lead to a change of the total magnetization of the field: the z components of spin of both interacting atoms remain unchanged, or the z component of one atom decreases by one while the z component of the second atom increases by one. The second line collects terms describing processes where both interacting atoms simultaneously flip the z-axis projection of their spin: both by $+1$ or both by -1. Notice that the respective terms are multiplied by the phase factor $e^{-2i\phi}$ or $e^{2i\phi}$. This corresponds to a change of the projection of the orbital angular momentum of atoms in their center of mass frame by -2 or 2 quanta. The last two lines describe processes in which the spin of one interacting atom is unchanged while the z-axis component of the spin of the other atom changes by $+1$ (or by -1). This spin flipping term is multiplied by the phase factor $e^{-i\phi}$ (or $e^{i\phi}$), which signifies the change of the z projection of relative orbital angular momentum of interacting atoms by -1 (or $+1$, respectively). Evidently, the dipolar interactions conserve the z projection of the total angular momentum of interacting atoms.

III. EINSTEIN–DE HAAS EFFECT IN A PLAQUETTE

We study a system of $N = 4 \times 10^3$ ^{87}Rb atoms initially in the polarized $m_F = +1$ state and the ground state of the external potential. Because the occupation of this state is macroscopic, we describe the system by a spinor wave function satisfying the Gross-Pitaevskii (GP) equation. We therefore replace the field operator $\hat{\psi}(\mathbf{r})$ by the c-number spinor wave function $\psi(\mathbf{r}) = (\psi_+(\mathbf{r}), \psi_0(\mathbf{r}), \psi_-(\mathbf{r}))^T$. Standard optical lattices for rubidium atoms have site separations in the submicron regime. In such a geometry, and with the number of atoms considered here, the tunneling between sites is large even for barriers much larger than those accessible experimentally. However, it is possible to suppress the tunneling by using larger separations between microtraps. Large separations can be reached in various ways, for example, by varying the angle between the copropagating laser beams that create the periodic potential.

We solve the spinor GP equation with the nonlocal dipolar potential on a spatial grid of $32 \times 32 \times 16$ points. The spatial steps are $dx = dy = 0.25\ \mu$m and $dz = 0.5\ \mu$m, the wave vector is $k_0 = 0.74\ \mu\text{m}^{-1}$, and the axial confinement is given by $\hbar\omega_z/E_R = 0.32$, where $E_R = \hbar^2 k_0^2/2m$ is the single-photon

recoil energy. Note that at each site, the microtrap potential has a prolate shape due to the harmonic confinement in the xy plane being tight in comparison with the one along the z direction. Here, we assume that the radial harmonic confinement is absent ($\omega_\perp = 0$). We instantly turn on the magnetic field and monitor the resulting dynamics of the spinor wave function. The transfer of atoms to other Zeeman states strongly depends on the value of the external magnetic field and the geometry of the trap [17]. This transfer is possible only when the Zeeman energy compensates for the excitation energy. Therefore we have to adjust the value of the external magnetic field to the resonant value. For a given initial state there are many magnetic resonances [29]. We focus on the first resonance, corresponding to the smallest value of the magnetic field and the most efficient transfer of atoms to other Zeeman components. We start our simulations with a relatively low barrier between plaquette sites, $V_0 = 10E_R$. At a resonant magnetic field of $B = 0.075$ mG, the transfer of atoms to the $m_F = 0$ component reaches its maximum after about $t = 4$ s, and subsequently begins to decrease. We observe an oscillationlike behavior of the population at longer time scales if the magnetic field remains on. To check the stability of the dynamically created state, we switch off the magnetic field at the moment when the transfer is maximal. This way the dipolar interactions are tuned out of the resonance. Also, the spin-mixing contact term is small because the number of atoms in the $m_F = 0$ component is of the order of 100 only. Therefore, further dynamics looks stationary, at least on time scales of a few seconds. The population of the $m_F = -1$ component remains always very small, and we ignore it in the discussion that follows. We stress however, that all Zeeman components are present in our calculations. Analysis of the one-particle density matrix averaged over the z axis [30] indicates that all three components of the spinor wave function are coherent.

In Fig. 1 we present the density distribution and the phase of the $m_F = 0$ component. The atomic cloud is concentrated around two horizontal xy planes, one at $z = 1.3/k_0$ and the second at $z = -1.3/k_0$. In both planes the density is the same. The discrete symmetry of the plaquette is clearly visible—almost all atoms are located at the centers of the quadrants of the plaquette. The phase of the wave function is constant in each quadrant but is not constant over the entire plaquette: it jumps by $\pi/2$ between neighboring quadrants. As a result, the phase of the atomic wave function winds around by 2π around the plaquette center. Evidently, a singly quantized discrete vortex in the $m_F = 0$ component is present. The geometry of the final state proves that the discrete symmetry of the whole plaquette determines the dynamics of the Einstein–de Haas effect—it dominates the local axial symmetry of the individual sites.

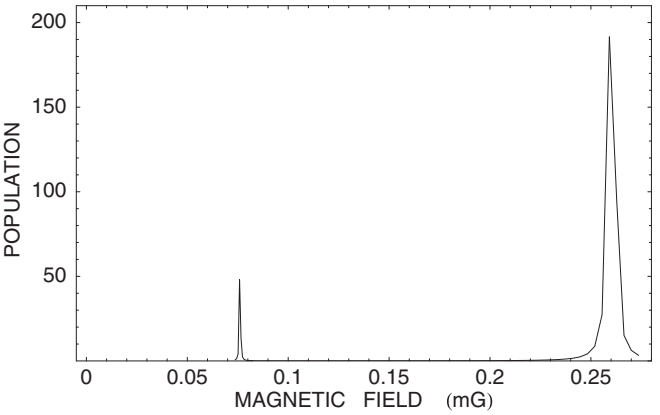

FIG. 2. Transfer of atoms to the $m_F = 0$ state as a function of the magnetic field for a plaquette with $V_0 = 10E_R$. Two resonances are visible. The one at the lower magnetic field corresponds to the case when the transfer of atoms is governed by the discrete symmetry of the plaquette (see Fig. 1). For the second resonance (at the higher magnetic field) the transfer to the $m_F = 0$ state occurs locally, at individual plaquette sites (see Fig. 3).

However, the topology of the final state can be changed. It turns out that there exists a resonance that populates a state with local vortices located at the lattice sites. To find such a resonance, we still keep the height of the barrier separating the sites at $V_0 = 10E_R$ but increase the magnetic field. We observe a significant transfer of atoms to the $m_F = 0$ state for a magnetic field equal to $B = 0.26$ mG (see Fig. 2). In Fig. 3 we show the density distribution of the $m_F = 0$ component at the maximum of the transfer. Similarly to the previous case, the final state does not change noticeably when evolved with the external magnetic field set to zero. The number of $m_F = 0$ atoms at each site is equal to $N_0 = 180$. We observe an array of singly quantized vortices. In each lattice site the density forms two rings—one above the $z = 0$ plane and a

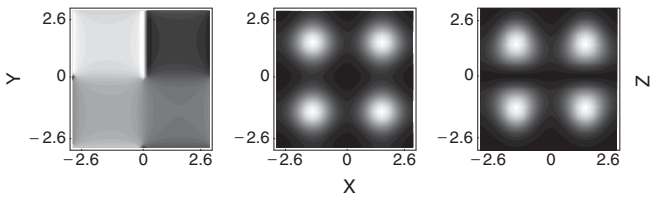

FIG. 1. Phase (left) and density (middle) in the xy plane at $z = 1.3/k_0$, and the density in the xz plane at $y = 1.5/k_0$ (right) of the $m_F = 0$ component at $t = 4$ s for $V_0 = 10E_R$ in the case without radial harmonic confinement. Here, $k_0 = 0.74\ \mu\text{m}^{-1}$ and the distance between lattice sites equals $d_0 = \pi/k_0 = 4.24\ \mu$m. The total number of atoms is $N = 4 \times 10^3$, and the resonant magnetic field is $B = 0.075$ mG. The maximal transfer to the $m_F = 0$ component is equal to $N_0 = 50$ atoms at $t = 4$ s.

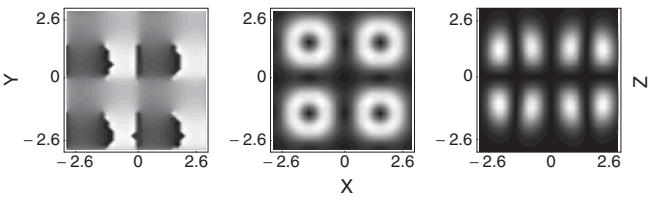

FIG. 3. Phase (left) and the density (middle) in the xy plane at $z = 1.3/k_0$, and the density in the xz plane at $y = 1.3/k_0$ (right) of the $m_F = 0$ component at $t = 4$ s for $V_0 = 10E_R$ in the case without radial harmonic confinement. Here, $k_0 = 0.74\ \mu\text{m}^{-1}$ and the distance between lattice sites equals $d_0 = \pi/k_0 = 4.24\ \mu$m. The total number of atoms is $N = 4 \times 10^3$, and the resonant magnetic field is $B = 0.26$ mG. The maximal transfer to the $m_F = 0$ component is equal to $N_0 = 180$ atoms at $t = 0.6$ s.

second one below this plane. The phase of the corresponding wave function winds around by 2π around every site center. Furthermore, the phases of individual vortices appear to be correlated, because lines where the phase is zero are parallel. Evidently, in the case of this resonance the transfer of atoms to the $m_F = 0$ component takes place locally, at every lattice site and resembles the Einstein–de Haas effect in an axially symmetric harmonic potential. Note that the potential in our case is only axially symmetric close to the potential minimum, at every site of the plaquette.

IV. FORMATION OF THE DISCRETE VORTEX AND LOCAL VORTEX ARRAY STATES

To get a better understanding of our numerical results, let us limit our spinor wave function to a few relevant states only. At every site localized at $\boldsymbol{r}_i = (x_i, y_i, 0)$ where $i = 1, \ldots, 4$ (for 2×2 plaquette), we keep only the ground state in the $m_F = 1$ component:

$$\langle \boldsymbol{r}|i\rangle_g = \mathcal{N}_0 \mathcal{W}_0(x - x_i, y - y_i) e^{-\beta z^2/4}. \tag{9}$$

Two-body dipolar interactions can transfer only one particle from the initial ground state $\langle \boldsymbol{r}|i\rangle_g$ to excited states with $m_F = 0$. Simultaneous transfer of both particles is strongly suppressed for large initial state occupations [29]. There are two relevant low energy excited states $\langle \boldsymbol{r}|i\rangle_{e_1}$ and $\langle \boldsymbol{r}|i\rangle_{e_2}$ in a given site which can be resonantly populated. The first one is the state with no orbital angular momentum and one z-excitation quantum:

$$\langle \boldsymbol{r}|i\rangle_{e_1} = \mathcal{N}_1 \mathcal{W}_0(x - x_i, y - y_i) z e^{-\beta z^2/4}, \tag{10}$$

while the second one has one quanta of orbital angular momentum and one z-excitation quantum:

$$\langle \boldsymbol{r}|i\rangle_{e_2} = \mathcal{N}_2 \mathcal{W}_1(x - x_i, y - y_i) z e^{-\beta z^2/4}. \tag{11}$$

$\mathcal{W}_0(x,y)$ is the two-dimensional Wannier ground-state wave function with zero orbital angular momentum. It is a product of one-dimensional Wannier ground states $\mathcal{W}_0(x,y) = W_0(x)W_0(y)$ while $\mathcal{W}_1(x,y) = [W_1(x)W_0(y) + iW_0(x)W_1(y)]/\sqrt{2}$ is the excited 2D Wannier state with one quantum of orbital angular momentum along the z axis. Here W_1 is the first excited 1D Wannier state, $\beta = \hbar\omega_z/E_R$ is the harmonic oscillator energy expressed in units of the recoil energy, while $\mathcal{N}_0$, $\mathcal{N}_1$, $\mathcal{N}_2$ are normalization constants. For a large occupation of the initial state, the processes leading to the chosen excited states strongly dominate over others, as was discussed in [29]. We will neglect the $m_F = -1$ component because its occupation is due to a second-order perturbation in dipolar interactions. The first excited state (10) could, in principle, be responsible for the appearance of the discrete vortex in the entire plaquette, while the second one (11) corresponds to the vortex array.

The mean energies of all the above states do not depend on the lattice site, and they are E_g, E_{e_1}, and E_{e_2}, respectively. All the states, i.e., the ground and the two excited states, are fourfold degenerate in the 2×2 plaquette. However, tunneling couples neighboring sites and partially removes this degeneracy. In the chosen basis the spectrum of the single-particle Hamiltonian splits into three "bands" of four Bloch states:

$$|\downarrow\rangle_\alpha = \tfrac{1}{2}(|1\rangle_\alpha + |2\rangle_\alpha + |3\rangle_\alpha + |4\rangle_\alpha), \tag{12a}$$

$$|\circlearrowleft\rangle_\alpha = \tfrac{1}{2}(|1\rangle_\alpha + i|2\rangle_\alpha - |3\rangle_\alpha - i|4\rangle_\alpha), \tag{12b}$$

$$|\circlearrowright\rangle_\alpha = \tfrac{1}{2}(|1\rangle_\alpha - i|2\rangle_\alpha - |3\rangle_\alpha + i|4\rangle_\alpha), \tag{12c}$$

$$|\uparrow\rangle_\alpha = \tfrac{1}{2}(|1\rangle_\alpha - |2\rangle_\alpha + |3\rangle_\alpha - |4\rangle_\alpha), \tag{12d}$$

where $\alpha = g, e_1, e_2$ and the state vector $|i\rangle_\alpha$ corresponds to the wave function $\langle \boldsymbol{r}|i\rangle_\alpha$. Energies of the four states within a given band are equal to $\{E_\alpha - 2J_\alpha, E_\alpha, E_\alpha, E_\alpha + 2J_\alpha\}$, respectively.

Tunneling coefficients in the ground band and in the first excited band are positive and equal, $J_g = J_{e_1}$, because all states in these bands have the same spatial profile in the xy plane. Therefore the states $|\downarrow\rangle_g$ and $|\downarrow\rangle_{e_1}$ are the lowest energy states in the corresponding bands. Tunneling between vortex states in the second excited band is negative, $J_{e_2} < 0$. Therefore the lowest energy state in this band is antiferromagnetic $|\uparrow\rangle_{e_2}$ with alternating relative phases rather than the ferromagnetic one $|\downarrow\rangle_{e_2}$. The subspace of eigenenergy E_α spanned by vectors $|\circlearrowleft\rangle_\alpha$ and $|\circlearrowright\rangle_\alpha$ is two dimensional, so one can choose any combination of these vectors as the basis. We choose the particular combination above since such vectors are not only the eigenstates of the Hamiltonian, but they are also those eigenstates that belong to the proper representations of the C_4 symmetry group with nonzero eigenvalues ± 1, i.e., they are closely related to the eigenstates of the angular momentum operator in the continuous system.

In our numerical simulations we prepared the system in the $|\downarrow\rangle_g$ state. Dipolar interactions can couple this state to both excited bands. The strength of this coupling is given by the two-body dipolar matrix element between the initial and final two-particle states. In the final state, one atom remains in the initial state, but the second one occupies one of the states from the excited bands. Direct evaluation of the relevant integrals shows that two of them strongly dominate the rest (by several orders of magnitude). One corresponds to the process when one atom is transferred to the discrete vortex state in the first excited band, i.e., the state in which the density profile is almost the same as in the initial state, but the phase changes from site to site by $\pi/2$:

$$|\downarrow\rangle_g \to |\circlearrowleft\rangle_{e_1} = \tfrac{1}{2}(|1\rangle_{e_1} + i|2\rangle_{e_1} - |3\rangle_{e_1} - i|4\rangle_{e_1}), \tag{13}$$

while the other transfers to the state with the array of four vortices:

$$|\downarrow\rangle_g \to |\downarrow\rangle_{e_2} = \tfrac{1}{2}(|1\rangle_{e_2} + |2\rangle_{e_2} + |3\rangle_{e_2} + |4\rangle_{e_2}). \tag{14}$$

The energy difference for the first process is $\delta E_1 = E_{e_1} - E_g + 2J_g$ while for the second one is $\delta E_2 = (E_{e_2} - E_g) - 2(J_{e_2} - J_g)$. Evidently the resonant value of the magnetic field for the first process is smaller than for the second one. Moreover, in the case of the second resonance the relative phases of vortices created at individual lattice sites are the same as relative phases in the initial state. The phase between vortices at different lattice sites is inherited from the initial state. If the initial state is $|\uparrow\rangle_g$, then atoms are transferred to the analogous state in the second excited band, $|\uparrow\rangle_{e_2}$.

This observation agrees very well with our numerical results presented in the previous section.

Now it is clear that the transfer of angular momentum from the spin part to the spatial part due to the dipolar interactions can be realized in two ways: by exciting particles in every site to the second excited band with an array of vortices, e_2, or by transferring particles to the first excited band—not changing the local density but changing the relative phases between plaquette sites, e_1.

The exact values of these two relevant dipolar transition amplitudes depend on the barrier height and the strength of confinement in the z direction (parameter β). For a deep enough lattice, since the sites become more symmetric, the transition to on-site vortices should dominate over the transition to a discrete vortex in the plaquette. On the other hand, when the lattice is shallow the on-site Wannier states with a vortex are quite different from the eigenfunctions of the "local" (at a given site) orbital angular momentum operators. Moreover the state with the discrete vortex, due to a high tunneling rate, becomes almost invariant under rotation around the center of the plaquette by an arbitrary angle (up to a phase factor). Therefore, we expect that the transition to the plaquette vortex will be dominant in this case. We have confirmed all these predictions by numerical calculations of dipolar transition amplitudes. The results are presented in Fig. 4. The parameter β which characterizes the trapping potential affects both the values of the transition amplitudes as well as the height of the barrier at which they cross. We would like to emphasize again that initial amplitudes which do not conserve the total angular momentum are numerically many orders smaller than those considered above.

The model presented above is in a very good qualitative agreement with the results of our numerical experiment. However, the values of the magnetic field for which the population in the discrete vortex dominates the population in the vortex array state are different. This is due to the simplifications we have made to get a clear picture of the relevant processes. In particular, the contact interactions were totally ignored. Their role is to change both the energies and the spatial spread of the atomic states, and this inevitably leads to quantitative differences.

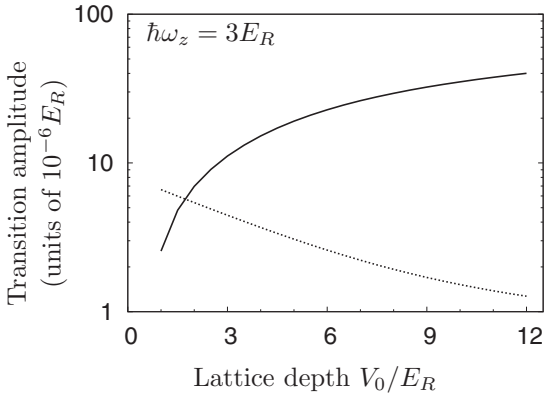

FIG. 4. Transition amplitudes induced by dipolar interactions for the 2×2 plaquette with $\hbar\omega_z/E_R = 3 = \beta$. For deeper lattices, the transition to the four independent vortices located at lattice sites (solid line) always dominates over the transition to the discrete vortex (dotted line).

V. STABILITY OF TOPOLOGICAL STATES

Now, we are going to investigate the stability of the states populated by the resonant Einstein–de Haas effect. For this purpose, we must turn on the radial harmonic confinement because study of the stability of discrete vortex and local vortices states requires that we first remove the optical potential and next restore it.

As a preliminary, we checked that we are able to find the same kinds of resonances as in Sec. III, when the radial harmonic confinement is present together with the periodic potential. Indeed, the presence of an extra radial harmonic potential results in a small shift of the resonant magnetic field and a small change in the number of atoms transformed to the $m_F = 0$ state, as compared to the cases discussed in Sec. III. For example, with an optical trap with $V_0 = 10E_R$ for the resonance which populates the singly quantized discrete vortex in the $m_F = 0$ component, we find that the resonant magnetic field equals $B = 0.08$ mG and the number of transferred atoms is $N_0 = 80$. For further studies we will now focus on the resonance just mentioned and one other which leads to a significant occupation of vortex states at individual plaquette sites. That one occurs for parameters $V_0 = 20E_R$, $B_{\text{res}} = 0.85$ mG, and $N_0 = 160$.

Depending on the barrier separating lattice sites and the value of the external magnetic field, the resonant dipolar interactions drive the system toward states of a different geometry. It is interesting to check if these states are robust against a perturbation of the trapping potential of the lattice. To this end we ramp the lattice potential down adiabatically to zero and then raise it back to the initial value, for both cases studied. The sequence of pictures in Figs. 5 and 6 shows how the density and the phase of the $m_F = 0$ component changes while the microtrap barrier is first lowered and then raised

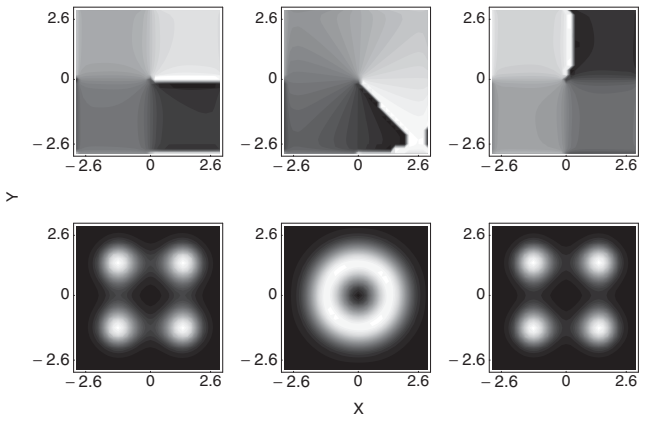

FIG. 5. Sequence of images of the phase (upper panel) and the density (lower panel) in the xy plane ($z = 1.3/k_0$) of the $m_F = 0$ component during lowering and raising of the barrier separating the microtraps: $V_0 = 10E_R$ (left), $V_0 = 0E_R$ (middle), and $V_0 = 10E_R$ (right). The barrier was lowered linearly in the time during $t = 0.5$ s. The images in the middle column are shown at 0.15 s after the barrier is removed. Subsequently the barrier was raised back in a further 1 s, and the initial configuration was recovered (right).

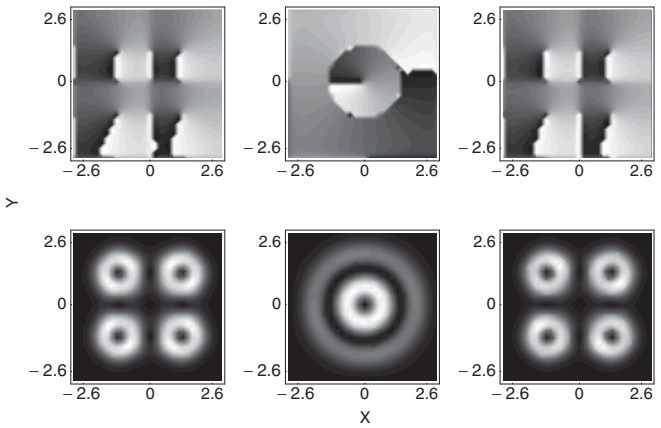

FIG. 6. Sequence of images as in Fig. 5, but for $V_0 = 20E_R, 0E_R$, and $20E_R$ (left, middle, and right, respectively). The images in the middle column are shown at 0.15 s after the barrier is removed. Then the barrier was raised back in a further 1 s, and the initial configuration was recovered right).

back. The lowering process lasts for $t = 0.5$ s. The middle columns show the density and the phase at 0.15 s after the barrier height reached zero. We see that in both cases atoms form a vortex around the center of the plaquette. In the case of a high initial barrier an additional ring of relatively low density surrounding the first one can be seen, as in Fig. 6. However, after raising the barrier back, both initial configurations are recovered (see the right columns of Figs. 5 and 6). This indicates that the initial states are essentially different and one cannot switch between these states after they are created.

To understand this difference let us examine the spatial structure of phases of both states in detail. Consider the initial states created via dipolar interactions at $t = 0$ shown in Fig. 7. The phase of the $m_F = 0$ state created at $V_0 = 10E_R$ has only one singular point. However, a much richer structure can be observed for the array of vortices obtained at $V_0 = 20E_R$ (left panel). In addition to the four singly quantized vortices

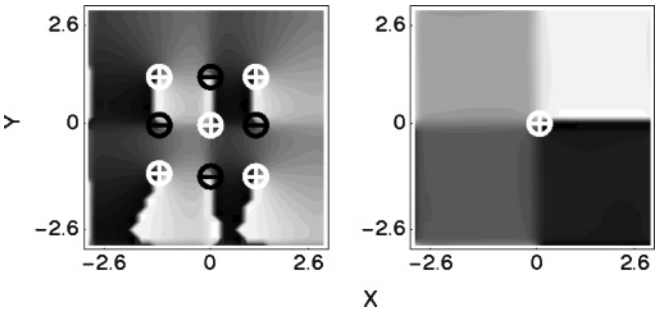

FIG. 7. Phase portraits of the $m_F = 0$ component obtained initially at $V_0 = 20E_R$ (left) and $V_0 = 10E_R$ (right). Notice a singly quantized discrete vortex of positive charge in the $V_0 = 10E_R$ case. For $V_0 = 20E_R$ there are five more vortices in addition to the four singly quantized vortices of positive topological charge located at the center of each quadrant where the atomic density is large. One of the extra five is located at the plaquette center, and the other four have the opposite topological charge and are located at the bonds connecting lattice minima. These additional five vortices are hidden in the region of a very low atomic density. The vortices and their charges are marked by white and black circles.

of positive topological charge located at the center of each minimum, there is one more vortex of the same charge located at the plaquette center and four more vortices of opposite topological charge. These vortices and their charges are marked by white and black circles in Fig. 7. These additional vortices are not seen in Fig. 6 because they are located in a region of very low density. However, numerical evaluation of circulation around every point of the grid allows us to detect them. The number of vortices strongly differentiates these two states. The vortex structures are stable against perturbation of the lattice potential; therefore it is not possible to switch between them by changing the intertrap barrier. The system recovers the initial symmetry even after the barrier was removed. This memory effect is due to a different number of vortices in both studied states. These two states belong to a particular representation of the C_4 point-symmetry group. This representation is characterized by the presence of a singly quantized vortex at the center of the plaquette. It is worth to note at this point that an extensive discussion of solutions of the GP equation belonging to different representations of the C_n point-symmetry group can be found in Ref. [31].

We would like to stress that our findings might be important for the observation of the Einstein–de Haas effect in optical lattices. Some experimental effort has been already taken in this direction [27]. Our results show that the properties of the rotating states created via the Einstein–de Haas effect strongly depend on the geometry of the trapping potential and the value of the external magnetic field.

VI. CONCLUSIONS

In conclusion, we have studied the formation of topological states via resonant dipolar interactions. We have paid particular attention to the competition between the local axial symmetry of the individual microtrap and the global discrete symmetry of the entire plaquette. We have shown that the role of these two symmetries can vary depending on the height of the intertrap barrier. For shallow enough plaquettes when the mean-field wave function penetrates the whole plaquette, a single discrete vortex is created. In the opposite case of weak tunneling, the transfer of atoms has a local character and the axial symmetry of individual sites allows the formation of an array of vortices located at each plaquette site. However, for a wide range of intermediate lattice depths, both kinds of topological states can be populated depending on the value of the applied magnetic field. These topological states are created dynamically with the help of the resonant Einstein–de Haas effect. Moreover, the vortex structures present in both states make them very stable against perturbations of the lattice potential. Even when the discrete symmetry of the plaquette is destroyed by removing the lattice potential, the system comes back to the initial configuration after the lattice potential is raised back.

ACKNOWLEDGMENTS

The work was supported by the UE project NAME-QUAM and the Polish Ministry for Science and Education for 2009–2011.

[1] J. Kronjäger, C. Becker, P. Navez, K. Bongs, and K. Sengstock, Phys. Rev. Lett. **97**, 110404 (2006); M. Erhard *et al.*, Phys. Rev. A **70**, 031602(R) (2004).

[2] M. S. Chang, C. D. Hamley, M. D. Barrett, J. A. Sauer, K. M. Fortier, W. Zhang, L. You, and M. S. Chapman, Phys. Rev. Lett. **92**, 140403 (2004).

[3] J. Mur-Petit, M. Guilleumas, A. Polls, A. Sanpera, M. Lewenstein, K. Bongs, and K. Sengstock, Phys. Rev. A **73**, 013629 (2006).

[4] H. Saito, Y. Kawaguchi, and M. Ueda, Phys. Rev. Lett. **96**, 065302 (2006).

[5] K. Gawryluk, M. Brewczyk, M. Gajda, and K. Rzążewski, Phys. Rev. A **76**, 013616 (2007).

[6] T. Świsłocki, M. Brewczyk, M. Gajda, and K. Rzążewski, Phys. Rev. A **81**, 033604 (2010).

[7] K. Góral, K. Rzążewski, and T. Pfau, Phys. Rev. A **61**, 051601(R) (2000).

[8] J.-P. Martikainen, M. Mackie, and K.-A. Suominen, Phys. Rev. A **64**, 037601 (2001).

[9] L. Santos, G. V. Shlyapnikov, and M. Lewenstein, Phys. Rev. Lett. **90**, 250403 (2003).

[10] A. Griesmaier, J. Werner, S. Hensler, J. Stuhler, and T. Pfau, Phys. Rev. Lett. **94**, 160401 (2005).

[11] Q. Beaufils, R. Chicireanu, T. Zanon, B. Laburthe-Tolra, E. Marechal, L. Vernac, J. C. Keller, and O. Gorceix, Phys. Rev. A **77**, 061601 (2008).

[12] T. Lahaye *et al.*, Rep. Prog. Phys. **72**, 126401 (2009).

[13] M. Ueda and Y. Kawaguchi, e-print arXiv:1001.2072v2.

[14] M. Vengalattore, S. R. Leslie, J. Guzman, and D. M. Stamper-Kurn, Phys. Rev. Lett. **100**, 170403 (2008).

[15] Y. Kawaguchi, H. Saito, and M. Ueda, Phys. Rev. Lett. **98**, 110406 (2007).

[16] S. Yi and H. Pu, Phys. Rev. Lett. **97**, 020401 (2006).

[17] K. Gawryluk, M. Brewczyk, K. Bongs, and M. Gajda, Phys. Rev. Lett. **99**, 130401 (2007).

[18] K. Gawryluk, K. Bongs, and M. Brewczyk, Phys. Rev. Lett. **106**, 140403 (2011).

[19] Y. Kawaguchi, H. Saito, and M. Ueda, Phys. Rev. Lett. **96**, 080405 (2006); L. Santos and T. Pfau, *ibid.* **96**, 190404 (2006).

[20] M. Greiner *et al.*, Nature (London) **415**, 39 (2002).

[21] T. Stoferle, H. Moritz, C. Schori, M. Kohl, and T. Esslinger, Phys. Rev. Lett. **92**, 130403 (2004).

[22] I. B. Spielman, W. D. Phillips, and J. V. Porto, Phys. Rev. Lett. **98**, 080404 (2007).

[23] I. Bloch, J. Dalibard, and W. Zwerger, Rev. Mod. Phys. **80**, 885 (2008).

[24] M. Lewenstein *et al.*, Adv. Phys. **56**, 243 (2007).

[25] J. Kruse, C. Gierl, M. Schlosser, and G. Birkl, Phys. Rev. A **81**, 060308(R) (2010).

[26] B. Pasquiou, G. Bismut, Q. Beaufils, A. Crubellier, E. Marechal, P. Pedri, L. Vernac, O. Gorceix, and B. Laburthe-Tolra, Phys. Rev. A **81**, 042716 (2010).

[27] B. Pasquiou, G. Bismut, E. Marechal, P. Pedri, L. Vernac, O. Gorceix, and B. Laburthe-Tolra, Phys. Rev. Lett. **106**, 015301 (2011).

[28] T.-L. Ho, Phys. Rev. Lett. **81**, 742 (1998); T. Ohmi and K. Machida, J. Phys. Soc. Jpn. **67**, 1822 (1998).

[29] T. Świsłocki, T. Sowiński, J. Pietraszewicz, M. Brewczyk, M. Lewenstein, J. Zakrzewski, and M. Gajda, Phys. Rev. A **83**, 063617 (2011).

[30] M. Brewczyk, M. Gajda, and K. Rzążewski, J. Phys. B **40**, R1 (2007).

[31] A. Ferrando, M. Zacarés, and M.-Á. García-March, Phys. Rev. Lett. **95**, 043901 (2005); M.-Á. García-March, A. Ferrando, M. Zacares, S. Sahu, and D. E. Ceballos-Herrera, Phys. Rev. A **79**, 053820 (2009).